Chapter 4
Classical Cyclotron

Abstract This chapter introduces to the classical cyclotron, and to the theoretical material needed for the simulation exercises. It begins with a brief reminder of the historical context, and continues with beam optics and acceleration techniques which the classical cyclotron principle and methods lean on, including
- ion orbit in a cyclic accelerator,
- weak focusing and periodic transverse motion,
- revolution period and isochronism,
- voltage gap and resonant acceleration,
- the cyclotron equation.

The simulation of a cyclotron dipole will either resort to an analytical model of the field: the optical element DIPOLE, or will resort to using a field map together with the keyword TOSCA to handle it and raytrace through. An additional accelerator device needed in the exercises, CAVITE, simulates a local oscillating voltage. Running a simulation generates a variety of output files, including the execution listing zgoubi.res, always, and other zgoubi.plt, zgoubi.CAVITE.out, zgoubi.MATRIX.out, etc., aimed at looking up program execution, storing data for post-treatment, producing graphs, etc. Additional keywords are introduced as needed, such as FIT[2], a matching procedure; FAISCEAU and FAISTORE which log local particle data in zgoubi.res or in a user defined ancillary file; MARKER; the 'system call' command SYSTEM; REBELOTE, a 'do loop'; and some more. This chapter introduces in addition to spin motion in accelerator magnets; dedicated simulation exercises include a variety of keywords: SPNTRK, a request for spin tracking, SPNPRT or FAISTORE, to log spin vector components in respectively zgoubi.res or some ancillary file, and the "IL=2" flag to log stepwise particle data, including spin vector, in zgoubi.plt file. Simulations include deriving transport matrices, beam matrix, optical functions and their transport, from rays, using MATRIX and TWISS keywords.

Notations used in the Text

B; B_0	field value; at reference radius R_0
$\mathbf{B}$; B_R; B_y	field vector; radial component; axial component
$BR = p/q$	magnetic rigidity
C; C_0	orbit length, $C = 2\pi R$; reference, $C_0 = 2\pi R_0$
E	ion energy
$f_{\rm rev}$, $f_{\rm rf}$	revolution and accelerating voltage frequencies
h	harmonic number, an integer, $h = f_{\rm rf}/f_{\rm rev}$
$k = \frac{R}{B}\frac{dB}{dR}$	radial field index
m; m_0; M	mass, $m = \gamma m_0$; rest mass; in units of MeV/c^2
$\mathbf{p}$; p; p_0	ion momentum vector; its modulus; reference
q	ion charge
R; R_0; R_E	orbit radius; reference radius $R(p_0)$; at energy E
RF	Radio-Frequency: as per the accelerating voltage technology
s	path variable
$T_{\rm rev}$, $T_{\rm rf}$	revolution and accelerating voltage periods
$\mathbf{v}$; v	ion velocity vector; its modulus
$V(t)$; $\hat{V}$	oscillating voltage; its peak value
W	kinetic energy, $W = \frac{1}{2}mv^2$
x, x', y, y'	radial and axial coordinates in the moving frame $[(*)' = d(*)/ds]$
α	momentum compaction
α	trajectory deviation
$\beta = v/c$; β_0; β_s	normalized ion velocity; reference; synchronous
$\gamma = E/m_0$	Lorentz relativistic factor
Δp, δp	momentum offset
ε_u	Courant-Snyder invariant ($u: \ x, r, y, l, Y, Z, s$, etc.)
θ	azimuthal angle
ϕ	RF phase at ion arrival at the voltage gap

4.1 Introduction

Cyclotrons are the most widespread type of accelerator, today, used by hundreds, with dominant application the production of isotopes. This chapter is devoted to the first cyclic accelerator: the 1930s "classical" cyclotron which its concept limited to low energy, a few 10s of MeV/nucleon, a limitation overcome a decade later by the azimuthally varying field (AVF) technique - subject of the next chapter.

The 1930s cyclotron is based on two main principles:
(i) resonant acceleration by synchronization of a fixed-frequency accelerating voltage on the quasi-constant revolution time, the very acceleration technique universally used a century later, and
(ii) transverse beam confinement based on so-called weak focusing, a technique

which would be used over the years in all (but the AVF) cyclic accelerators: cyclotron, microtron, betatron, synchrotron, until the invention of alternating gradient strong focusing in the early 1950s; weak focusing it is still in use today, in betatrons and low energy proton synchrotrons mostly.

Resonant acceleration had the great advantage that a small gap voltage is enough to accelerate with, in principle, no energy limitation, by contrast with the electrostatic techniques developed at the time which required the generation of the full voltage, such as the Van de Graaf limited for this reason at a few tens of MeV.

The cyclotron concept goes back to the late 1920s [1], a cyclotron was first brought to operation in the early 1930s [2], its principles are summarized in Fig. 4.1: an oscillating voltage is applied on a pair of electrodes ("dees") forming an accelerating gap and placed between the two poles of an electromagnet; ions reaching the gap during the acceleration phase of the voltage wave experience an energy boost; under the effect of energy increase, they spiral out in the quasi-constant field of the dipole. The first cyclotron achieved acceleration of H_2^+ hydrogen ions to 80 keV [2], at

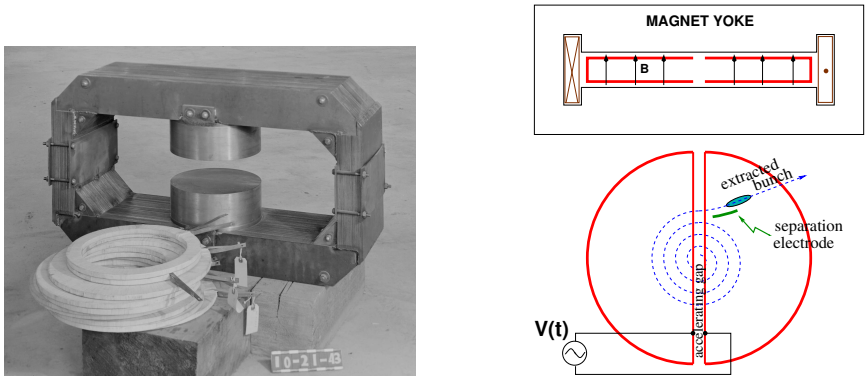

Fig. 4.1 Left: dipole electromagnet used for a model of Berkeley's 184-inch cyclotron, in 1943 [3]. Right: a schematic view of the resonant acceleration method: in the uniform field between the two cylindrical magnetic poles (top), accelerated ions spiral out (bottom); a double-dee (or, a variant, a single-dee facing a slotted electrode) forms a gap to which is applied a fixed-frequency oscillating voltage $V(t)$ of which the frequency is a harmonic of the revolution frequency; ions experiencing proper voltage phase at the gap are accelerated; a septum electrode allows beam extraction

Berkeley in 1931. The apparatus used a dee-shaped electrode vis-à-vis a slotted electrode forming a voltage gap, the ensemble housed in a 5 in diameter vacuum chamber and placed in the 1.3 Tesla field of an electromagnet. A $\approx$ 12 MHz vacuum tube oscillator provided a 1 kVolt gap voltage.

One goal foreseen in developing this technology was the acceleration of protons to MeV energy range for the study of atom nucleus - and in background a wealth of potential applications. An 11 in cyclotron followed which delivered a 0.01 μA H_2^+ beam at 1.22 MeV [4], and a 27 in cyclotron later reached 6 MeV (Fig. 4.2) [5]. Targets were mounted at the periphery of the 11-inch cyclotron, disintegrations were

observed in 1932. And, in 1933: *'The neutron had been identified by Chadwick in* 1932. *By* 1933 *we were producing and observing neutrons from every target bombarded by deuterons."* [5, M.S. Livingston, p. 22].

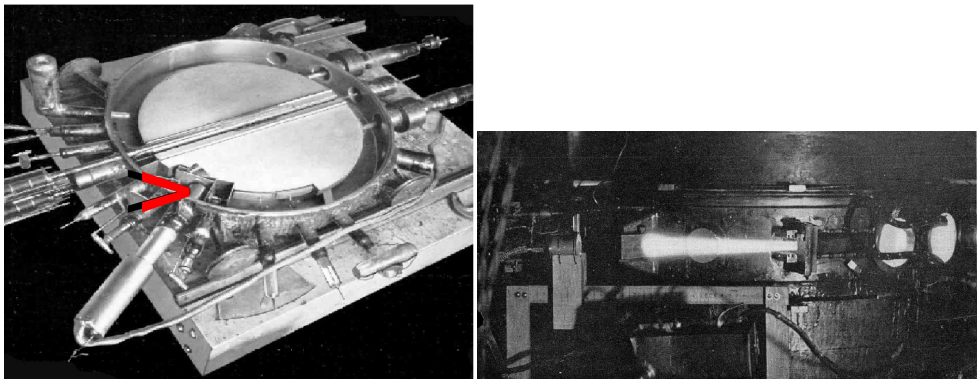

Fig. 4.2 Berkeley 27-inch cyclotron, brought to operation in 1934, accelerated deuterons up to 6 MeV. Left: a double-dee (seen in the vacuum chamber, cover off), 22 in diameter, creates an accelerating gap: 13 kV, 12 MHz radio frequency voltage is applied for deuterons for instance (through two feed lines seen at the right). This apparatus was dipped in the 1.6 Tesla dipole field of a 27 in diameter, 75 ton, electromagnet. A slight decrease of the dipole field with radius, from the center of the dipole, ensures axial beam focusing. With their energy increasing, ions spiral out from the center to eventually strike a target (arrow). Right: ionization of the air by the extracted beam (1936); the view also shows the vacuum chamber squeezed between the pole pieces of the electromagnet [3]

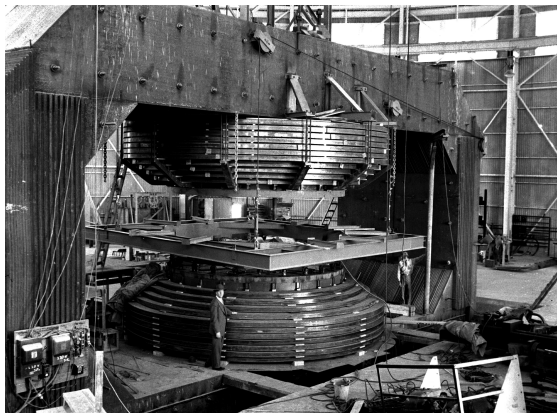

Fig. 4.3 Berkeley 184 in diameter, 4,000 ton cyclotron during construction [3]. Its design was modified and it was operated as a synchrocyclotron from the beginning, in 1946

A broad range of applications were foreseen: *"At this time biological experiments were started.* [...] *Also at about this same time the first radioactive tracer experiments on human beings were tried* [...] *simple beginnings of therapeutic use, coming a*

little bit later, in which neutron radiation was used, for instance, in the treatment of cancer. [...] *Another highlight from* 1936 *was the first time that anyone tried to make artificially a naturally occurring radio-nuclide.* (*a bismuth isotope*) [5, McMillan, p. 26].

Limitation in energy

A complete understanding of ion dynamics in the classical cyclotron took more or less until the mid-1930s and brought two news, a bad one and a good one,

(i) bad one first: the energy limitation, a consequence of the loss of isochronism resulting from the relativistic increase of the ion mass so that "[...] *it seems useless to build cyclotrons of larger proportions than the existing ones* [...] *an accelerating chamber of* 37 *in radius will suffice to produce deuterons of* 11 *MeV energy which is the highest possible* [...]" [6], or in a different form: "*If you went to graduate school in the* 1940*s, this inequality* ($-1 < k < 0$) *was the end of the discussion of accelerator theory*" [7].

(ii) the good news now: the overcoming of the energy limit which results from the mass increase, by splitting the magnetic pole into valley and hill field sectors: the azimuthally varying field (AVF) cyclotron, by L.H. Thomas in 1938 [8] - the object of Chapt. 5. It took some years to see effects of this breakthrough.

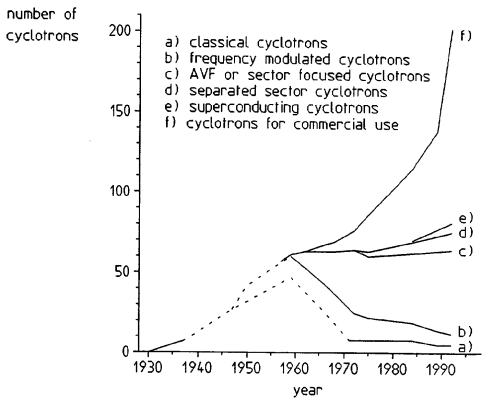

Fig. 4.4 Evolution of the number of the various cyclotron species, over the years [9] [10, Fig. 8]. From the 1950s on the AVF cyclotron rapidly supplanted the 1930s' classical cyclotron

With the progress in magnet computation tools, in computational speed and beam dynamics simulations, the AVF cyclotron ends up being essentially as simple to design and build has in a general manner supplanted the classical cyclotron in all energy domains (Fig. 4.4).

4.2 Basic Concepts and Formulæ

The cyclotron was conceived as a means to overcome the technological difficulty of a long series of high electrostatic voltage electrodes in a linear layout, by, instead, repeated recirculation through a single accelerating gap in synchronism with an oscillating voltage (Fig. 4.5). With its energy increasing, an accelerated bunch spirals

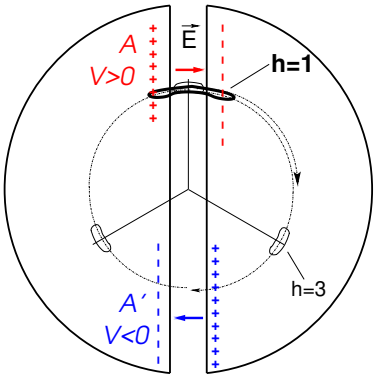

Fig. 4.5 Resonant acceleration: in an $h = 1$ configuration an ion bunch meets an oscillating field **E** across gap A, at time t, on accelerating phase; it meets again, half a turn later, at time $t + T_{\rm rev}/2$, the accelerating phase across gap A', and so on: the uniform magnetic field recirculates the bunch through the gap, repeatedly. Higher harmonic allows more bunches: the next possibility with two dees is h=3, and 3 bunches, 120 degrees apart, in synchronism with **E**

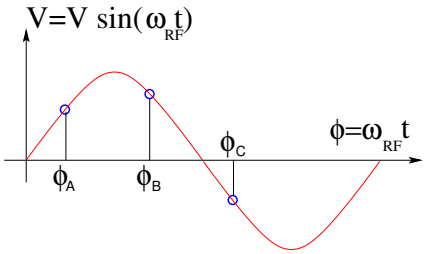

Fig. 4.6 A ion which reaches the double-dee gap at the RF phase $\omega_{\rm rf}t = \phi_A$ or $\omega_{\rm rf}t = \phi_B$ is accelerated. If it reaches the gap at $\omega_{\rm rf}t = \phi_C$ it is decelerated

out in the uniform magnetic field, the velocity increase comes with an increase in orbit length; the net result is a slow increase of the revolution period $T_{\rm rev}$ with energy, yet, with appropriate fixed voltage frequency $f_{\rm rf} \approx h/T_{\rm rev}$ the revolution motion and the oscillating voltage can be maintained in sufficiently close synchronism, $T_{\rm rev} \approx hT_{\rm rf}$, that the bunch will transit the voltage gap upon accelerating phase (Fig. 4.6) over a large enough number of turns that it acquires a significant energy boost.

The orbital motion quantities: radius R, ion rigidity BR, revolution frequency $f_{\rm rev}$, satisfy

$$BR = \frac{p}{q}, \qquad 2\pi f_{\rm rev} = \omega_{\rm rev} = \frac{v}{R} = \frac{qB}{m} = \frac{qB}{\gamma m_0} \tag{4.1}$$

relationships which hold at all γ, so covering the *classical* cyclotron domain ($v \ll c$, $\gamma \approx 1$) as well as the *isochronous* cyclotron (ion energy increase commensurate with its mass - Chapt. 5). To give an idea of the revolution frequency, in the limit $\gamma = 1$, for protons, one has $f_{\rm rev}/B = q/2\pi m = 15.25\,{\rm MHz/T}$.

The cyclotron design sets the constant RF frequency $f_{\rm rf} = \omega_{\rm rf}/2\pi$ at an intermediate value of $h f_{\rm rev}$ along the acceleration cycle. The energy gain, or loss, by the ion when transiting the gap, at time t, is

$$\Delta W(t) = q\hat{V}\sin\phi(t) \quad \text{with} \quad \phi(t) = \omega_{\rm rf}t - \omega_{\rm rev}t + \phi_0 \tag{4.2}$$

with ϕ its phase with respect to the RF signal at the gap (Fig. 4.6), $\phi_0 = \phi(t = 0)$, and $\omega_{\rm rev}t$ the orbital angle. Assuming constant field B, the increase of the revolution period with ion energy satisfies

$$\frac{\Delta T_{\rm rev}}{T_{\rm rev}} = \gamma - 1$$

The mis-match so induced between the RF and cyclotron frequencies is a turn-by-turn cumulative effect and sets a limit to the tolerable isochronism defect, $\Delta T_{\rm rev}/T_{\rm rev} \approx 2 - 3\%$, or highest velocity $\beta = v/c \approx 0.22$. This results for instance in a practical limitation to $\approx 25\,{\rm MeV}$ for protons, and $\approx 50\,{\rm MeV}$ for D and α particles.

Over time multiple-gap accelerating structures where developed, whereby a "multiple-Δ" electrode pattern substitutes a "double-D". An example is GANIL C0 injector with its 4 accelerating gaps and $h = 4$ and $h = 8$ RF harmonic operation [11].

4.2.1 Fixed-Energy Orbits, Revolution Period

In a laboratory frame (O;x,y,z), with (O;x,z) the bend plane (Fig. 4.7), assume $\mathbf{B}|_{y=0} = \mathbf{B}_y$, constant. An ion is launched from the origin with a velocity

$$\mathbf{v} = \left(\frac{dx}{dt}, \frac{dy}{dt}, \frac{dz}{dt}\right) = (v\sin\alpha, 0, v\cos\alpha)$$

at an angle α from the z-axis.

Solving

$$m\dot{\mathbf{v}} = q\mathbf{v}\times\mathbf{B} \tag{4.3}$$

with $\mathbf{B} = (0, B_y, 0)$ yields the parametric equations of motion

$$\begin{cases} x(t) = \dfrac{v}{\omega_{\rm rev}}\cos(\omega_{\rm rev}t - \alpha) - \dfrac{v\cos\alpha}{\omega_{\rm rev}} \\ y(t) = \text{constantz(t)} = \dfrac{\rm v}{\omega_{\rm rev}}\sin(\omega_{\rm rev}{\rm t} - \alpha) + \dfrac{\rm v\sin\alpha}{\omega_{\rm rev}} \end{cases} \tag{4.4}$$

which result in

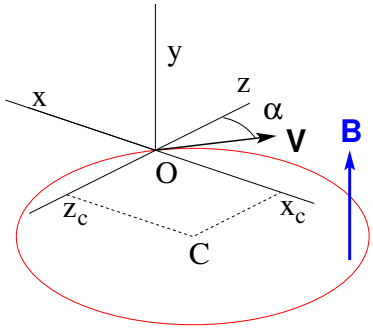

Fig. 4.7 Circular motion of an ion in the plane normal to a uniform magnetic field **B**. The orbit is centered at $x_C = -v\cos\alpha/\omega_{\rm rev}$, $z_C = v\sin\alpha/\omega_{\rm rev}$, its radius is $v/\omega_{\rm rev}$

$$\left(x + \frac{v\cos\alpha}{\omega_{\rm rev}}\right)^2 + \left(z - \frac{v\sin\alpha}{\omega_{\rm rev}}\right)^2 = \left(\frac{v}{\omega_{\rm rev}}\right)^2 \tag{4.5}$$

a circular trajectory of radius $R = v/\omega_{\rm rev}$ centered at $(x_C, z_C) = (-\frac{v\cos\alpha}{\omega_{\rm rev}}, \frac{v\sin\alpha}{\omega_{\rm rev}})$.

Stability of the cyclic motion - The initial velocity vector defines a, say "reference", closed orbit in the median plane of the cyclotron dipole; a small perturbation in α or v defines a new orbit *in the vicinity* of the reference. An axial velocity component v_y on the other hand, causes the ion to drift away from the reference, vertically, linearly with time, as there is no axial restoring force. The next Section will investigate the necessary field property to ensure both horizontal and vertical confinement of the cyclic motion in the vicinity of a reference orbit in the median plane.

4.2.2 Weak Focusing

In the early accelerated turns in a classical cyclotron (central region of the electromagnet, energy up to tens of keV/u), the accelerating electric field provides adequate transverse focusing [11], whereas a flat magnetic field with uniformity $dB/B < 10^{-4}$ is sufficient to maintain isochronism. Beyond this low energy region however, at greater radii, a magnetic field gradient must be introduced to ensure transverse stability: field must decrease with R.

Ion coordinates in the following are defined in the moving frame $(M_0; s, x, y)$ (Fig. 4.8), which moves along the reference orbit (radius R_0), with its origin M_0 the projection of ion location M on the reference orbit; the s axis is tangent to the latter, the x axis is normal to s, the y axis is normal to the bend plane. Median-plane symmetry of the field is assumed, thus the radial field component $B_R|_{y=0} = 0$ at all R (Fig. 4.9).

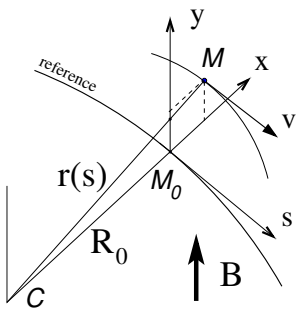

Fig. 4.8 Moving frame $(M_0; s, x, y, s)$ along the reference circular orbit. The curvature $1/R_0$ is constant along the orbit and $(M_0; s, x, y)$ can be considered equivalent to the cylindrical frame $(C; \theta, R_0, y)$

Consider small motion excursions from $(R = R_0, y = 0)$: $x(t) = R(t) - R_0 \ll R_0$; introduce the Taylor expansion of the vertical field component

$$B_y(R_0 + x) = B_y(R_0) + x \left.\frac{\partial B_y}{\partial R}\right|_{R_0} + \frac{x^2}{2!} \left.\frac{\partial^2 B_y}{\partial R^2}\right|_{R_0} + \ldots \approx B_y(R_0) + x \left.\frac{\partial B_y}{\partial R}\right|_{R_0}$$

$$B_R(0 + y) = y \underbrace{\left.\frac{\partial B_R}{\partial y}\right|_0}_{= \left.\frac{\partial B_y}{\partial R}\right|_{R_0}} + \frac{y^3}{3!} \left.\frac{\partial^3 B_R}{\partial y^3}\right|_0 + \ldots \approx y \left.\frac{\partial B_y}{\partial R}\right|_{R_0} \tag{4.6}$$

Using these, and noting $\dot{(*)} = d(*)/dt$, the linear approximation of the differential equations of motion in the moving frame writes

$$F_x = m\ddot{x} = -qvB_y(R) + \frac{mv^2}{R_0 + x} \approx -qv \left(B_y(R_0) + \left.\frac{\partial B_y}{\partial R}\right|_{R_0} x \right) + \frac{mv^2}{R_0} \left(1 - \frac{x}{R_0}\right)$$

$$\rightarrow m\ddot{x} = -\frac{mv^2}{R_0^2} \left(\frac{R_0}{B_0} \left.\frac{\partial B_y}{\partial R}\right|_{R_0} + 1 \right) x \tag{4.7}$$

$$F_y = m\ddot{y} = qvB_R(y) = qv \left.\frac{\partial B_R}{\partial y}\right|_{y=0} y + \text{higher order} \rightarrow m\ddot{y} = qv \frac{\partial B_y}{\partial R} y$$

Note $B_y(R_0) = B_0$ and introduce

$$\omega_R^2 = \omega_{\text{rev}}^2 \left(1 + \frac{R_0}{B_0} \frac{\partial B_y}{\partial R}\right), \quad \omega_y^2 = -\omega_{\text{rev}}^2 \frac{R_0}{B_0} \frac{\partial B_y}{\partial R} \tag{4.8}$$

substitute in Eqs. 4.7, this yields

$$\ddot{x} + \omega_{\mathrm{R}}^2 \mathrm{x} = 0 \qquad \text{and} \qquad \ddot{y} + \omega_{\mathrm{y}}^2 \mathrm{y} = 0 \tag{4.9}$$

A restoring force (linear terms in x and y, Eq. 4.9) arises from the radially varying field, characterized by a field index

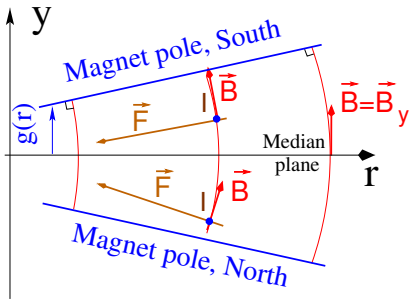

Fig. 4.9 Axial motion stability requires proper shaping of field lines: B_y has to decrease with radius. The Laplace force pulls a positive charge with velocity pointing out of the page, at I, toward the median plane. Increasing the field gradient (k closer to -1, gap opening up faster) increases the focusing

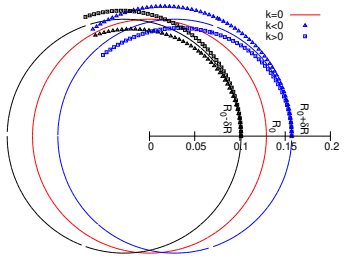

Fig. 4.10 Geometrical focusing: in a uniform field, k=0, the two circular trajectories which start from $r = R_0 \pm \delta R$ (solid lines, going counterclockwise) undergo exactly one oscillation around the reference orbit $r = R_0$. A negative k (triangles), a necessary condition for axial focusing, decreases the radial convergence; a positive k (square markers) increases the radial convergence - and increases vertical motion divergence

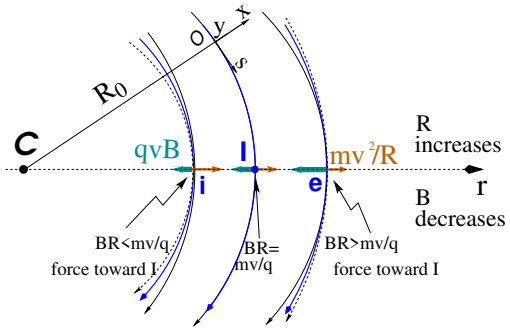

Fig. 4.11 Radial motion stability in an axially symmetric structure. Trajectories arcs at p=mv are represented: case of k=0 (thin black lines), of -1<k<0 (thick blue lines), and of k=-1 (dashed concentric circles). k decreasing towards -1 reduces the geometrical focusing, increases axial focusing. The resultant of the Laplace and centrifugal forces, $F_t = -qvB + mv^2/r$, is zero at I, motion is stable if F_t is toward I at i, *i.e.* $qvB_i < mv^2/R_i$, and toward I as well at e, *i.e.* $qvB_e > mv^2/R_e$

$$k = \frac{R_0}{B_0}\frac{\partial B_y}{\partial R}\bigg|_{R=R_0, y=0} \tag{4.10}$$

Radial stability - radially this force adds to the geometrical focusing (curvature term "1" in ω_R^2, Eq. 4.8, Fig. 4.10). In the weakly decreasing field $B(R)$ an ion with momentum $p = mv$ moving in the vicinity of the R_0-radius reference orbit experiences in the moving frame a resultant force $F_t = -qvB + m\frac{v^2}{r}$ (Fig. 4.11) of which the (outward) component $f_c = m\frac{v^2}{r}$ decreases with r at a higher rate than the decrease of the Laplace (inward) component $f_B = -qvB(r)$. In other words, radial stability requires BR to increase with R, $\frac{\partial BR}{\partial R} = B + R\frac{\partial B}{\partial R} > 0$, this holds in particular at R_0, thus $1 + k > 0$.

Axial stability requires a restoring force directed toward the median plane. Referring to Fig. 4.9, this means $F_y = -a \times y$ (with a a positive quantity) and thus $B_R < 0$, at all $(r, y \neq 0)$. This is achieved by designing a guiding field which decreases with radius, $\frac{\partial B_R}{\partial y} < 0$. Referring to Eq. 4.10 this means $k < 0$.

From these radial and axial constraints the condition of "weak focusing" for transverse motion stability around the circular equilibrium orbit results, namely,

$$-1 < k < 0 \tag{4.11}$$

Note regarding the geometrical focusing: the focal distance associated with the curvature of a magnet of arc length $\mathcal{L}$ is obtained by integrating $\frac{d^2x}{ds^2} + \frac{1}{R_0^2}x = 0$ and identifying with the focusing property $\Delta x' = -x/f$, namely,

$$\Delta x' = \int \frac{d^2x}{ds^2}ds \approx \frac{-x}{R^2}\int ds = \frac{-x\mathcal{L}}{R^2}, \text{ thus } f = \frac{R^2}{\mathcal{L}} \tag{4.12}$$

Isochronism: the axial focusing constraint: B deceasing with R, contributes breaking the isochronism (in addition to the effect of the mass increase) by virtue of $\omega_{\text{rev}} \propto B$.

Paraxial Transverse Coordinates

Introduce the path variable, s, as the independent variable in Eq. 4.9 and neglect the transverse velocity components: $ds \approx vdt$; the equations of motion in the moving frame (Eq. 4.9) thus take the form

$$\frac{\mathrm{d}^2\mathrm{x}}{\mathrm{ds}^2} + \frac{1+\mathrm{k}}{\mathrm{R}_0^2}\mathrm{x} = 0 \qquad \text{and} \qquad \frac{\mathrm{d}^2\mathrm{y}}{\mathrm{ds}^2} - \frac{\mathrm{k}}{\mathrm{R}_0^2}\mathrm{y} = 0 \tag{4.13}$$

Given $-1 < k < 0$ the motion is that of a harmonic oscillator, in both planes, with respective restoring constants $(1 + k)/R_0^2$ and $-k/R_0^2$, both positive quantities. The solution is a sinusoidal motion,

$$\begin{cases} R(s) - R_0 = x(s) = \mathrm{x_0} \cos \frac{\sqrt{1+\mathrm{k}}}{\mathrm{R_0}}(\mathrm{s}-\mathrm{s_0}) + \mathrm{x'_0} \frac{\mathrm{R_0}}{\sqrt{1+\mathrm{k}}} \sin \frac{\sqrt{1+\mathrm{k}}}{\mathrm{R_0}}(\mathrm{s}-\mathrm{s_0}) \\ R'(s) = x'(s) = -\mathrm{x_0} \frac{\sqrt{1+\mathrm{k}}}{\mathrm{R_0}} \sin \frac{\sqrt{1+\mathrm{k}}}{\mathrm{R_0}}(\mathrm{s}-\mathrm{s_0}) + \mathrm{x'_0} \cos \frac{\sqrt{1+\mathrm{k}}}{\mathrm{R_0}}(\mathrm{s}-\mathrm{s_0}) \end{cases} \tag{4.14}$$

$$\begin{cases} \mathrm{y(s)} = \mathrm{y_0} \cos \frac{\sqrt{-\mathrm{k}}}{\mathrm{R_0}}(\mathrm{s}-\mathrm{s_0}) + \mathrm{y'_0} \frac{\mathrm{R_0}}{\sqrt{-\mathrm{k}}} \sin \frac{\sqrt{-\mathrm{k}}}{\mathrm{R_0}}(\mathrm{s}-\mathrm{s_0}) \\ \mathrm{y'(s)} = -\mathrm{y_0} \frac{\sqrt{-\mathrm{k}}}{\mathrm{R_0}} \sin \frac{\sqrt{-\mathrm{k}}}{\mathrm{R_0}}(\mathrm{s}-\mathrm{s_0}) + \mathrm{y'_0} \cos \frac{\sqrt{-\mathrm{k}}}{\mathrm{R_0}}(\mathrm{s}-\mathrm{s_0}) \end{cases} \tag{4.15}$$

Radial and axial wave numbers can be introduced,

$$\nu_R = \frac{\omega_R}{\omega_{\mathrm{rev}}} = \sqrt{1+k} \quad \text{and} \quad \nu_y = \frac{\omega_y}{\omega_{\mathrm{rev}}} = \sqrt{-k} \tag{4.16}$$

i.e., the number of sinusoidal oscillations of the paraxial motion about the reference circular orbit over a turn, respectively radial and axial. Both are less than 1: there is less than one sinusoidal oscillation in a revolution. In addition, as a result of the axial symmetry,

$$\nu_R^2 + \nu_y^2 = 1 \tag{4.17}$$

Off-Momentum Motion

In an axially symmetric structure, the equilibrium trajectory at momentum $\begin{cases} \mathrm{p_0} \\ \mathrm{p} = \mathrm{p_0} + \Delta\mathrm{p} \end{cases}$ is at radius $\begin{cases} \mathrm{R_0 \text{ such that } B_0 R_0 = p_0/q} \\ \mathrm{R \text{ such that } BR = p/q} \end{cases}$, with $\begin{cases} \mathrm{B} = \mathrm{B_0} + \left(\frac{\partial \mathrm{B}}{\partial \mathrm{x}}\right)_0 \Delta\mathrm{x} + \ldots \\ \mathrm{R} = \mathrm{R_0} + \Delta\mathrm{x} \end{cases}$

On the other hand

$$BR = \frac{p}{q} \Rightarrow \left[B_0 + \left(\frac{\partial B}{\partial x}\right)_0 \Delta x + \ldots\right](R_0 + \Delta x) = \frac{p_0 + \Delta p}{q}$$

which, neglecting terms in $(\Delta x)^2$, and given $B_0 R_0 = \frac{p_0}{q}$, leaves $\Delta x \left[\left(\frac{\partial B}{\partial x}\right)_0 R_0 + B_0\right] = \frac{\Delta p}{q}$. With $k = \frac{R_0}{B_0}\left(\frac{\partial B}{\partial x}\right)_0$ this yields

$$\Delta x = D\,\frac{\Delta p}{p_0} \qquad \text{with} \qquad D = \frac{R_0}{1+k} \quad \text{the dispersion function} \tag{4.18}$$

The dispersion D is an s-independent quantity as a result of the cylindrical symmetry of the field (k and R=p/qB are s-independent).

To the first order in the coordinates, the vertical coordinates y(s), y'(s) (Eq. 4.15) are unchanged under the effect of a momentum offset, the horizontal trajectory angle x'(s) (Eq. 4.14) is unchanged as well (the circular orbits are concentric, Fig. 4.12) whereas $x(s)$ satisfies

$$\mathrm{x(s, p_0 + \Delta p)} = \mathrm{x(s, p_0)} + \Delta\mathrm{p}\left.\frac{\partial \mathrm{x}}{\partial \mathrm{p}}\right|_{\mathrm{s,p_0}} = \mathrm{x(s, p_o)} + \mathrm{D}\frac{\Delta \mathrm{p}}{\mathrm{p_0}} \tag{4.19}$$

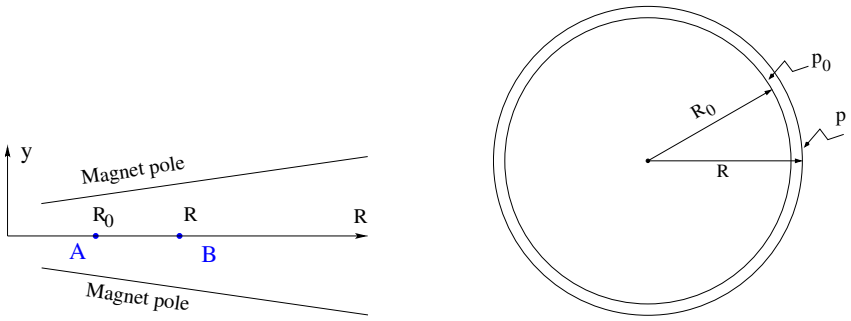

Fig. 4.12 The equilibrium radius at location A is R_0, the equilibrium momentum is p_0, rigidity is B_0R_0. The equilibrium radius at B is R, equilibrium momentum p, rigidity BR

Orbit and revolution period lengthening

A $p + \delta p$ off-momentum motion satisfies (Eq. 4.18)

$$\frac{\delta C}{C} = \frac{\delta R}{R} = \frac{\delta x}{R} = \alpha \frac{\delta p}{p} \quad \text{with} \quad \alpha = \frac{1}{1+k} = \frac{1}{\nu_R^2} \tag{4.20}$$

with α the "momentum compaction", a positive quantity: orbit length increases with momentum. Substituting $\frac{\delta\beta}{\beta} = \frac{1}{\gamma^2}\frac{\delta p}{p}$, the change in revolution period $T_{\text{rev}} = C/\beta c$ with momentum writes

$$\frac{\delta T_{\text{rev}}}{T_{\text{rev}}} = \frac{\delta C}{C} - \frac{\delta\beta}{\beta} = \left(\alpha - \frac{1}{\gamma^2}\right)\frac{\delta p}{p} \tag{4.21}$$

Given that $-1 < k < 0$ and $\gamma \gtrsim 1$, it results that $\alpha - 1/\gamma^2 > 0$: the revolution period increases with energy, the increase in radius is faster than the velocity increase.

4.2.3 Quasi-Isochronous Resonant Acceleration

The energy W of an accelerated ion (in the non-relativistic energy domain, which is that of the classical cyclotron) satisfies the frequency dependence

$$W = \frac{1}{2}mv^2 = \frac{1}{2}m\left(2\pi R f_{\text{rev}}\right)^2 = \frac{1}{2}m\left(2\pi R\frac{f_{\text{rf}}}{h}\right)^2 \tag{4.22}$$

Observe in passing: given the cyclotron size (radius R), f_{rf} and h set the limit for the acceleration range. The revolution frequency decreases with energy and the condition of synchronism with the oscillating voltage, $f_{\text{rf}} = hf_{\text{rev}}$, is only fulfilled at that particular radius where $\omega_{\text{rf}} = qB/m$ (Fig. 4.13-left). The out-phasing $\Delta\phi$ of the RF at ion arrival at the gap builds-up turn after turn, decreasing in a first stage

(towards lower voltages in Fig. 4.13-right) and then increasing back to $\phi = \pi/2$ and beyond towards π. Beyond $\phi = \pi$ the RF voltage is decelerating.

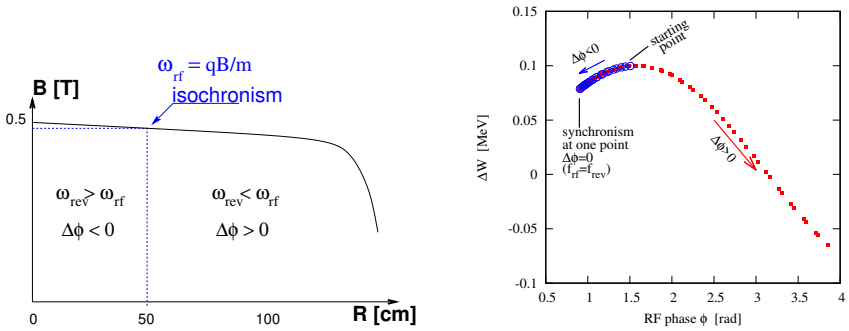

Fig. 4.13 Left: a sketch of the synchronism condition at one point (h=1 assumed). Right: the span in phase of the energy gain $\Delta W = q\hat{V}\sin\phi$ (Eq. 4.2) over the acceleration cycle

With $\omega_{\rm rev}$ constant between two gap passages, differentiating $\phi(t)$ (Eq. 4.2) yields $\dot{\phi} = \omega_{\rm rf} - \omega_{\rm rev}$. Between two gap passages on the other hand, $\Delta\phi = \dot{\phi}\Delta T = \dot{\phi}T_{\rm rev}/2 = \dot{\phi}\frac{\pi R}{v}$, yielding a phase-shift of

$$\text{half-turn} \quad \Delta\phi = \pi\left(\frac{\omega_{\rm rf}}{\omega_{\rm rev}(R)} - 1\right) = \pi\left(\frac{m\omega_{\rm rf}}{qB(R)} - 1\right) \tag{4.23}$$

The out-phasing is thus a gap-after-gap, cumulative effect. Due to this the classical cyclotron requires quick acceleration (limited number of turns), which means high voltage (tens to hundreds of kVolts). As expected, with $\omega_{\rm rf}$ and B constant, ϕ presents a minimum ($\dot{\phi} = 0$) at $\omega_{\rm rf} = \omega_{\rm rev} = qB/m$ where exact isochronism is reached (Fig. 4.13). The upper limit to ϕ is set by the condition $\Delta W > 0$: acceleration.

The cyclotron equation determines the achievable energy range, depending on the injection energy E_i, the RF phase at injection ϕ_i, the RF frequency $\omega_{\rm rf}$ and gap voltage $\hat{V}$, and writes [12]

$$\cos\phi = \cos\phi_i + \pi\left[1 - \frac{\omega_{\rm rf}}{\omega_{\rm rev}}\frac{E + E_i}{2M}\right]\frac{E - E_i}{q\hat{V}} \tag{4.24}$$

and is represented in Fig. 4.14 for various values of the peak voltage and phase at injection ϕ_i. M [eV/c^2] and E [eV] are respectively the rest mass and relativistic energy, $q\hat{V}$ is expressed in electron-volts, the index i denotes injection parameters.

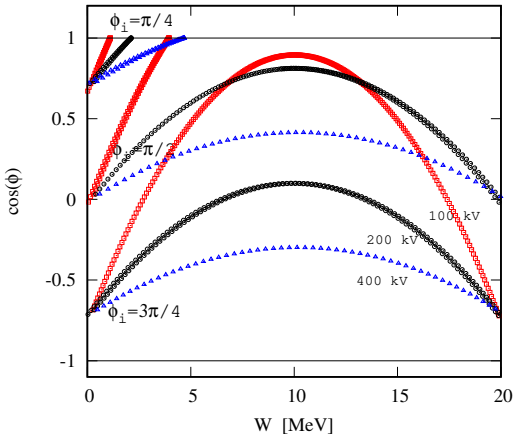

Fig. 4.14 A graph of the cyclotron equation (Eq. 4.24), for three different accelerating voltage settings: 100, 200 and 400 kV/gap (respectively square, circle and triangle markers). The sole settings resulting in $-1 < \cos\phi(E) < 1$, $\forall E$, allow complete acceleration to top energy. $\phi_i = \pi/4$ at injection for instance, does not allow acceleration to 20 MeV (upper three curves). Acceleration to 20 MeV works for $\phi_i = 3\pi/4$ (lower three curves), with as low as 100 kV/gap

4.2.4 Beam Extraction

From $R = p/qB$ and assuming $B(R) \approx$constant (this is legitimate as k is normally small), in the non-relativistic approximation ($W \ll M$, $W = p^2/2M$) one gets

$$\frac{dR}{R} = \frac{1}{2}\frac{dW}{W} \tag{4.25}$$

Integrating yields

$$R^2 = R_i^2 \frac{W}{W_i} \tag{4.26}$$

with R_i, W_i initial conditions. From Eqs. 4.25, 4.26, assuming $W_i \ll W$ and constant acceleration rate dW such that $W = n\,dW$ after n turns, one gets the scaling laws

$$R \propto \sqrt{n}, \qquad dR \propto \frac{R}{W} \propto \frac{1}{R} \propto dW, \qquad \frac{dR}{dn} = \frac{R}{2n} \tag{4.27}$$

Thus, in particular, the turn separation dR/dn is proportional to the orbit radius R and to the energy gain per turn.

The radial distance between successive turns decreases with energy, toward zero (Fig. 4.15), eventually resulting in insufficient spacing for insertion of an extraction septum.

Orbit modulation

Consider an ion bunch injected in the cyclotron with some (x_0, x_0') conditions in the vicinity of the reference orbit, and assume very slow acceleration. While accelerated the bunch undergoes an oscillatory motion around the local closed orbit (Eq. 4.14).

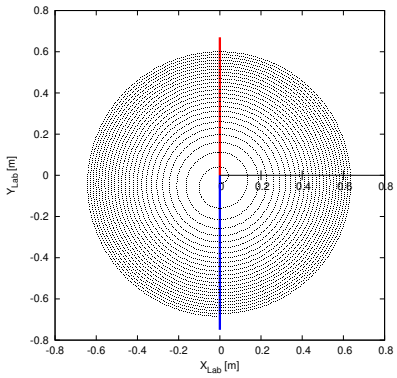

Fig. 4.15 The radial distance between successive turns decreases with energy, in inverse proportion to the orbit radius. The red and blue segments here figure the accelerting gap

Observed at the extraction septum this oscillation modulates the distance of the bunch to the local reference closed orbit, moving it outwards or inwards depending on the turn number, which modulates the distance between the accelerated turns. This effect can be exploited to increase the separation between the final two turns and so enhance the extraction efficiency [9].

4.2.5 Spin Dance

The magnetic field **B** of the cyclotron dipole exerts a torque on the spin angular momentum **S** of an ion, causing it to precess following the Thomas-BMT differential equation [13]

$$\frac{d\mathbf{S}}{dt} = \mathbf{S} \times \underbrace{\frac{q}{m}\left[(1+G)\mathbf{B}_{\parallel} + (1+G\gamma)\mathbf{B}_{\perp}\right]}_{\boldsymbol{\omega}_{\mathrm{sp}}} \tag{4.28}$$

wherein t is the time; $\boldsymbol{\omega}_{\mathrm{sp}}$ the precession vector: a combination of $\mathbf{B}_{\parallel}$ and $\mathbf{B}_{\perp}$ components of **B** respectively parallel and orthogonal to the ion velocity vector. G is the gyromagnetic anomaly,

G=1.7928474 (proton), -0.178 (Li), -0.143 (deuteron), -4.184 (^{3}He) ...

S in this equation is in the ion rest frame, all other quantities are in the laboratory frame.

In the case of an ion moving in the median plane of the dipole, $\mathbf{B}_{\parallel} = 0$, thus the precession axis is parallel to the magnetic field vector, $\mathbf{B}_y$, so that $\boldsymbol{\omega}_{\mathrm{sp}} = \frac{q}{m}(1 + G\gamma)\mathbf{B}_y$. The precession angle over a trajectory arc $\mathcal{L}$ is

$$\theta_{\mathrm{sp,\,Lab}} = \frac{1}{v}\int_{(\mathcal{L})} \omega_{\mathrm{sp}}\, ds = (1+G\gamma)\frac{\int_{(\mathcal{L})} B\, ds}{BR} = (1+G\gamma)\alpha \tag{4.29}$$

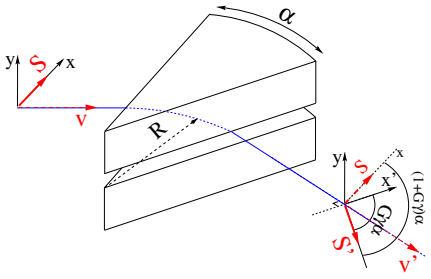

Fig. 4.16 Spin and velocity vector precession in a constant field, from **S** to **S′** and **v** to **v′** respectively. In the moving frame the spin precession along the arc $\mathcal{L} = R\alpha$ is $G\gamma\alpha$, in the laboratory frame the spin precesses by $(1 + G\gamma)\alpha$

with α the trajectory deviation angle (Fig. 4.16). The precession angle in the moving frame (the latter rotates by an angle α along $\mathcal{L}$) is

$$\theta_{\mathrm{sp}} = G\gamma\alpha \tag{4.30}$$

thus the number of 2π spin precessions per ion orbit around the cyclotron is $G\gamma$. By analogy with the wave numbers (Eq. 4.16) this defines the "spin tune"

$$\nu_{\mathrm{sp}} = G\gamma \tag{4.31}$$

4.3 Exercises

4.1 Modeling a Cyclotron Dipole: Using a Field Map

Solution: page 259

In this exercise, ion trajectories are ray-traced, various optical properties addressed in the foregoing are recovered, using a field map to simulate the cyclotron dipole. Fabricating that field map is a preliminary step of the exercise.

The interest of using a field map is that it is an easy way to account for fancy magnet geometries and fields, including field gradients and possible defects. A field map can be generated using mathematical field models, or from magnet computation codes, or from magnetic measurements. The first method is used, here. TOSCA keyword [14, *cf.* INDEX] is used to ray-trace through the map.

Working hypotheses: A 2-dimensional $m(R,\theta)$ polar meshing of the median plane is considered (Fig. 4.17). It is defined in a $(O;X,Y)$ frame and covers an angular sector of a few tens of degrees. The mid-plane field map is the set of values $B_Z(R,\theta)$ at the nodes of the mesh. During ray-tracing, TOSCA extrapolates the field along 3D space (R,θ,Z) ion trajectories from the 2D map [14].

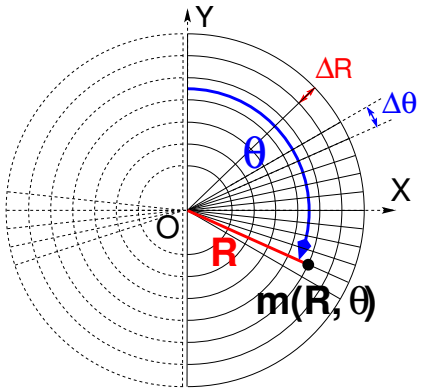

Fig. 4.17 Principle of a 2D field map in polar coordinates, covering a 180^o sector (over the right hand side dee). The mesh nodes $m(R,\theta)$ are distant ΔR radially, $\Delta\theta$ azimuthally. The map is used twice to cover the 360^o cyclotron dipole as sketched here, while allowing insertion of an accelerating gap between the two dees

(a) Construct a 180^o two-dimensional map of a median plane field $B_Z(R,\theta)$, proper to simulate the field in a cyclotron as sketched in Fig. 4.1. Use one of the following two methods: either (i) write an independent program, or (ii) use `zgoubi` and its analytical field model DIPOLE, together with the keyword CONSTY [14, *cf.* INDEX].

Besides: use a uniform mesh (Fig. 4.17) covering from Rmin=1 to Rmax=76 cm, with radial increment $\Delta R = 0.5$ cm, azimuthal increment $\Delta\theta = 0.5\,[\text{cm}]/R_0$ with R_0 some reference radius (say, 50 cm, in view of subsequent exercises), and constant axial field $B_Z = 0.5$ T. The appropriate 6-column formatting of the field map data for TOSCA to read is the following:

$$R\cos\theta,\ Z,\ R\sin\theta,\ BY,\ BZ,\ BX$$

with θ varying first, R varying second; Z is the vertical direction (normal to the map mesh), $Z \equiv 0$ in the present case. Note that proper functioning of TOSCA requires the field map to begin with the following line of numerical values:

Rmin [cm] ΔR [cm] $\Delta\theta$ [deg] Z [cm]

Produce a graph of the $B_Z(R, \theta)$ field map content.

(b) Ray-trace a few concentric circular mid-plane trajectories centered on the center of the dipole, ranging in $10 \leq R \leq 80$ cm. Produce a graph of these concentric trajectories in the $(O; X, Y)$ laboratory frame.

Initial coordinates can be defined using OBJET, particle coordinates along trajectories during the stepwise ray-tracing can be logged in zgoubi.plt by setting IL=2 under TOSCA. In order to find the Larmor radius corresponding to a particular momentum, the matching procedure FIT can be used. In order to repeat the latter for a series of different momenta, REBELOTE[IOPT=1] can be used.

Explain why it is possible to push the ray-tracing beyond the 76 cm radial extent of the field map.

(c) Compute the orbit radius R and the revolution period T_{rev} as a function of kinetic energy W or rigidity BR. Produce a graph, including for comparison the theoretical dependence of T_{rev}.

(d) Check the effect of the density of the mesh (the choice of ΔR and $\Delta\theta$ values, *i.e.*, the number of nodes $N_\theta \times N_R = (1 + \frac{180^o}{\Delta\theta}) \times (1 + \frac{80\,\text{cm}}{\Delta R})$), on the accuracy of the trajectory and time-of-flight computation.

(e) Consider a mesh with such ΔR, $\Delta\theta$ density as to ensure reasonably good convergence of the numerical resolution of the differential equation of motion [14, Eq. 1.2.4].

Check the effect of the integration step size on the accuracy of the trajectory and time-of-flight computation, by considering a small $\Delta s = 1$ cm and a large $\Delta s = 20$ cm, at 200 keV and 5 MeV (proton).

(f) Consider a periodic orbit, thus its radius R should remain unchanged after stepwise integration of the motion over a turn. However, the size Δs of the numerical integration step has an effect on the final value of the radius:

for two different cases, 200 keV (a small orbit) and 5 MeV (a larger one), provide the dependence of the relative error $\delta R/R$ after one turn, on the integration step size Δs (consider a series of Δs values in a range Δs : 0.1 mm $\rightarrow$ 20 cm). Provide a graph of the two $\frac{\delta R}{R}(\Delta s)$ curves (200 keV and 5 MeV).

4.2 Modeling a Cyclotron Dipole: Using an Analytical Field Model

Solution: page 267

This exercise is similar to exercise 4.1, yet using the analytical modeling DIPOLE, instead of a field map. DIPOLE provides the Z-parallel median plane field $\mathbf{B}(R, \theta, Z = 0) \equiv \mathbf{B}_Z(R, \theta, Z = 0)$ at the projected $m(R, \theta, Z = 0)$ ion location (Fig. 4.18), while $\mathbf{B}(R, \theta, Z)$ at particle location is obtained by extrapolation.

(a) Simulate a 180^o sector dipole; DIPOLE requires a reference radius [14, Eqs. 6.3.19-21], noted R_0 here; for the sake of consistency with other exercises, it is suggested to take $R_0 = 50$ cm. Take a constant axial field $B_Z = 0.5$ T.

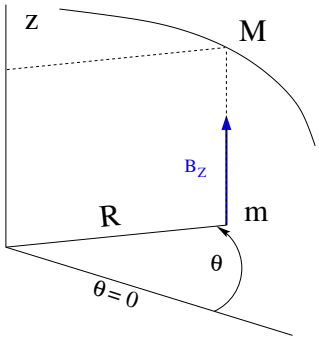

Fig. 4.18 DIPOLE provides the value $B_Z(m)$ of the median plane field at m, projection of particle position $M(R, \theta, Z)$ in the median plane. $\mathbf{B}(R, \theta, Z)$ is obtained by extrapolation

Explain the various data that define the field simulation in DIPOLE: geometry, role of R_0, field and field indices, fringe fields, integration step size, etc.

Produce a graph of $B_Z(R, \theta)$.

(b) Repeat question (b) of exercise 4.1.

(c) Repeat question (c) of exercise 4.1.

(d) As in question (e) of exercise 4.1, check the effect of the integration step size on the accuracy of the trajectory and time-of-flight computation.

Repeat question (f) of exercise 4.1.

(e) From the two series of results (exercise 4.1 and the present one), comment on various pros and cons of the two methods, field map versus analytical field model.

4.3 Resonant Acceleration

Solution: page 272

Based on the earlier exercises, using indifferently a field map (TOSCA) or an analytical model of the field (DIPOLE), introduce a sinusoidal voltage between the two dees, with peak value 100 kV. Assume that ion motion does not depend on RF phase: the boost through the gap is the same at all passes, use CAVITE[IOPT=3] [14, *cf.* INDEX] for that. Note that using CAVITE requires prior PARTICUL in order to specify ion species and data, necessary to compute the energy boost (Eq. 4.2).

(a) Accelerate a proton with initial kinetic energy 20 keV, up to 5 MeV, take harmonic h=1. Produce a graph of the accelerated trajectory in the laboratory frame.

(b) Provide a graph of the proton momentum p and total energy E as a function of its kinetic energy, both from this numerical experiment (ray-tracing data can be stored using FAISTORE) and from theory, all on the same graph.

(c) Provide a graph of the normalized velocity $\beta = v/c$ as a function of kinetic energy, both numerical and theoretical, and in the latter case both classical and relativistic.

(d) Provide a graph of the relative change in velocity $\Delta\beta/\beta$ and orbit length $\Delta C/C$ as a function of kinetic energy, both numerical and theoretical. From their evolution, conclude that the time of flight increases with energy.

(e) Repeat the previous questions, assuming a harmonic h=3 RF frequency.

4.4 Spin Dance

Solution: page 275

Cyclotron modeling in the present exercise can use Exercise 4.1 or Exercise 4.2 technique (*i.e.*, a field map or an analytical field model), indifferently.

(a) Add spin transport, using SPNTRK [14, *cf.* INDEX]. Produce a listing (zgoubi.res) of a simulation, including spin outcomes.

Note: PARTICUL is necessary here, for the spin equation of motion (Eq. 4.28) to be solved [14, Sect. 2]. SPNPRT can be used to have local spin coordinates listed in zgoubi.res (at the manner that FAISCEAU lists local particle coordinates).

(b) Consider proton case, take initial spin longitudinal, compute the spin precession over one revolution, as a function of energy over a range 12 keV→5 MeV. Give a graphical comparison with theory.

FAISTORE can be used to store local particle data, which include spin coordinates, in a zgoubi.fai style output file. IL=2 [14, *cf.* INDEX] (under DIPOLE or TOSCA, whichever modeling is used) can be used to obtain a print out of particle and spin motion data to zgoubi.plt during stepwise integration.

(c) Inject a proton with longitudinal initial spin $\mathbf{S}_i$. Give a graphic of the longitudinal spin component value as a function of azimuthal angle, over a few turns around the ring. Deduce the spin tune from this computation. Repeat for a couple of different energies.

Place both FAISCEAU and SPNPRT commands right after the first dipole sector, and use them to check the spin rotation and its relationship to particle rotation, right after the first passage through that first sector.

(d) Spin dance: the input data file optical sequence here is assumed to model a full turn. Inject an initial spin at an angle from the horizontal plane (this is in order to have a non-zero vertical component), produce a 3-D animation of the spin dance around the ring, over a few turns.

(e) Repeat questions (b-d) for two additional ions: deuteron (much slower spin precession), $^3He^{2+}$ (much faster spin precession).

4.5 Synchronized Spin Torque

Solution: page 281

A synchronized spin kick is superimposed on orbital motion. An input data file for a complete cyclotron is considered as in question 4.4 (d), for instance six 60 degree DIPOLEs, or two 180 degree DIPOLEs.

Insert a local spin rotation of a few degrees around the longitudinal axis, at the end of the optical sequence (*i.e.*, after one orbit around the cyclotron). SPINR can be used for that, to avoid any orbital effect. Track 4 particles on their closed orbit, with respective energies 0.2, 108.412, 118.878 and 160.746 MeV.

Produce a graph of the motion of the vertical spin component S_y along the circular orbit.

Produce a graph of the spin vector motion on a sphere.

4.6 Weak Focusing

Solution: page 285

(a) Consider a 60^o sector as in earlier exercises (building a field map and using TOSCA as in exercise 4.1, or using DIPOLE as in exercise 4.2), construct the sector accounting for a non-zero radial index k in order to introduce axial focusing, say $k = -0.03$, assume a reference radius R_0 for a reference energy of 200 keV (R_0 and B_0 are required in order to define the index k, Eq. 4.10). Ray-trace that 200 keV reference orbit, plot it in the lab frame: make sure it comes out as expected, namely, constant radius, final and initial angles zero.

(b) Find and plot the radius dependence of orbit rigidity, $BR(R)$, from ray-tracing over a BR range covering 20 keV to 5 MeV; superpose the theoretical curve. REBELOTE can be used to perform the scan.

(c) Produce a graph of the paraxial axial motion of a 1 MeV proton, over a few turns (use IL=2 under TOSCA, or DIPOLE, to have step by step particle and field data logged in zgoubi.plt). Check the effect of the focusing strength by comparing the trajectories for a few different index values, including close to -1 and close to 0.

(d) Produce a graph of the magnetic field experienced by the ion along these trajectories.

4.7 Loss of Isochronism

Solution: page 294

Compare on a common graphic the revolution period $T_{\rm rev}(R)$ for a field index value $k \approx -0.95,\ -0.5,\ -0.03,\ 0^-$. The scan method of exercise 4.6, based on REBELOTE, can be referred to.

4.8 Ion Trajectories

Solution: page 296

In this exercise individual ion trajectories are computed. DIPOLE or TOSCA magnetic field modeling can be used, indifferently. No acceleration here, ions cycle around the cyclotron at constant energy.

(a) Produce a graph of the horizontal and vertical trajectory components x(s) and y(s) of an ion with rigidity close to $BR(R_0)$ (R_0 is the reference radius in the definition of the index k), over a few turns around the cyclotron. From the number of turns, give an estimate of the wave numbers. Check the agreement with the expected $\nu_R(k)$, $\nu_y(k)$ values (Eq. 4.16).

(b) Consider now protons at 1 MeV and 5 MeV, far from the reference energy $E(R_0)$; the wave numbers change with energy: consistency with theory can be checked. Find their theoretical values, compare with numerical outcomes.

(c) Consider proton, 200 keV energy, plot as a function of s the difference between $x(s)$ from raytracing and its values from Eq. 4.14. Same for y(s) compared to Eq. 4.15. IL=2 can be used to store in zgoubi.plt the step-by-step particle coordinates across DIPOLE.

(d) Perform a scan of the wave numbers over 200 keV−5 MeV energy interval, computed using MATRIX, and using REBELOTE to repeat MATRIX for a series of energy values.

4.9 RF Phase at the Accelerating Gap

Solution: page 302

Consider the cyclotron model of exercise 4.6: field index $k = -0.03$ defined at $R_0 = 50\,\text{cm}$, field $B_0 = 5\,kG$ on that radius. two dees, double accelerating gap.

Accelerate a proton from 1 to 5 MeV: get the turn-by-turn phase-shift at the gaps; use CAVITE[IOPT=7] to simulate the acceleration. Compare the half-turn $\Delta\phi$ so obtained with the theoretical expectation (Eq. 4.23). Produce similar graphs $B(R)$ and $\Delta W(\phi)$ to Fig. 4.13.

Accelerate over more turns, observe the particle decelerating.

4.10 The Cyclotron Equation

Solution: page 304

The cyclotron model of exercise 4.3 is considered: two dees, double accelerating gap, uniform field $B = 0.5\,\text{T}$, no gradient.

(a) Set up an input data file for the simulation of a proton acceleration from 0.2 to 20 MeV. In particular, assume that $\cos(\phi)$ reaches its maximum value at $W_m = 10\,\text{MeV}$; find the RF voltage frequency from $d(\cos\phi)/dW = 0$ at W_m.

(b) Give a graph of the energy-phase relationship (Eq. 4.24), for $\phi_i = \frac{3\pi}{4},\ \frac{\pi}{2},\ \frac{\pi}{4}$, from both simulation and theory.

4.11 Cyclotron Extraction

Solution: page 306

(a) Acceleration of a proton in a uniform field B=0.5 T is first considered (field hypotheses as in exercise 4.3). RF phase is ignored: CAVITE[IOPT=3] can be used for acceleration. Take a 100 kV gap voltage.

Compute the distance ΔR between turns, as a function of turn number and of energy, over the range $E:\ 0.02 \rightarrow 5\,\text{MeV}$. Compare graphically with theoretical expectation.

(b) Assume a beam with Gaussian momentum distribution and *rms* momentum spread $\delta p/p = 10^{-3}$. An extraction septum is placed half-way between two successive turns, provide a graph of the percentage of beam loss at extraction, as a function of extraction turn number - COLLIMA can be used for that simulation and for particle counts, it also allows for possible septum thickness.

(c) Repeat (a) and (b) considering a field with index: take for instance $B_0 = 0.5\,\text{T}$ and $k = -0.03$ at $R_0 = R(0.2\,\text{MeV}) = 12.924888\,\text{cm}$.

(d) Investigate the effect of injection conditions (Y_i, T_i) on the modulation of the distance between turns.

Show numerically that, with slow acceleration, the oscillation is minimized for an initial $|T_i| = |\frac{x_0 \nu_R}{R}|$ (after Ref. [9, p. 133]).

4.12 Acceleration and Extraction of a 6-D Polarized Bunch

Solution: page 311

The cyclotron simulation hypotheses of exercise 4.10-a are considered.

Add a short "high energy" extraction line, say 1 meter, following REBELOTE in the optical sequence, ending up with a "Beam_Dump" MARKER for instance.

(a) Create a 1,000 ion bunch with the following initial parameters:

- random Gaussian transverse phase space densities, centered on the closed orbit, truncated at 3 sigma, normalized *rms* emittances $\varepsilon_Y = \varepsilon_Z = 1\,\pi\mu$m, both emittances matched to the 0.2 MeV orbit optics,
- uniform bunch momentum density $0.2\times(1-10^{-3}) \le p \le 0.2\times(1+10^{-3})$ MeV, matched to the dispersion, namely (Eq. 4.19), $\Delta x = D\frac{\Delta p}{p}$,
- random uniform longitudinal distribution $-0.5 \le s \le 0.5$ mm,

Note: two ways to create this object are, (i) using MCOBJET[KOBJ=3] which generates a random distribution, or (ii) using OBJET[KOBJ=3] to read an external particle coordinate file.

Add spin tracking request (SPNTRK), all initial spins normal to the bend plane.

Produce a graph of the three initial 2-D phase spaces: (Y,T), (Z,P), (δl,$\delta p/p$), matched to the 200 keV periodic optics. Provide Y, Z, dp/p, δl and S_Z histograms, check the distribution parameters.

(b) Accelerate this polarized bunch to 20 MeV, using the following RF conditions:

- 200 kV peak voltage,
- RF harmonic 1,
- initial RF phase $\phi_i = \pi/4$.

Produce a graph of the three phase spaces as observed downstream of the extraction line. Provide the Y, Z, dp/p, δl and S_Z histograms. Compare the distribution parameters with the initial values.

What causes the spins to spread away from vertical?

References

1. Jones, L., Mills, F., Sessler, A., et al.: Innovation Was Not Enough. World Scientific (2010)
2. Lawrence, E.O., Livingston, M.S. Phys. Rev. 37, 1707 (1931), 1707; Phys. Rev. 38, 136, (1931); Phys. Rev. 40, 19 (1932)
3. Credit: Lawrence Berkeley National Laboratory. ©The Regents of the University of California, Lawrence Berkeley National Laboratory
4. Lawrence, E.O. and Livingston, M.S.: The Production of High Speed Light Ions Without the Use of High Voltages. Phys. Rev. 40, 19-35 (1932)
5. Livingston, M.S., McMillan, E.M.: History of the cyclotron. Physics Today, 12(10) (1959). https://escholarship.org/uc/item/29c6p35w
6. Bethe, H. E., Rose, M. E.: Maximum energy obtainable from cyclotron. Phys. Rev. 52 (1937) 1254
7. Cole, F.T.: O Camelot ! A memoir of the MURA years (April 1, 1994). https://accelconf.web.cern.ch/c01/cyc2001/extra/Cole.pdf
8. 4.a Thomas, L.H.: The Paths of Ions in the Cyclotron. Phys. Rev. 54, 580, (1938) 4.b Craddock, M.K.: AG focusing in the Thomas cyclotron of 1938. Proceedings of PAC09, Vancouver, BC, Canada, FR5REP1
9. Stammbach, T.: Introduction to Cyclotrons. CERN accelerator school, cyclotrons, linacs and their applications. IBM International Education Centre, La Hulpe, Belgium, 28 April-5 May 1994
10. Credit: CERN Accelerator School. Stammbach, T.: Introduction to Cyclotrons. CERN Yellow Report 96-02 (1996), Figure 8, page 15, unchanged. Copyright/License CERN CC-BY-3.0 - https://creativecommons.org/licenses/by/3.0
11. Baron, E., et al.: The GANIL Injector. Proceedings of the 7th International Conference on Cyclotrons and their Applications, Zürich, Switzerland (1975). http://accelconf.web.cern.ch/c75/papers/b-05.pdf
12. Le Duff, J.: Longitudinal beam dynamics in circular accelerators. CERN Accelerator School, Jyvaskyla, Finland, 7-18 September 1992
13. Méot, F.: Spin Dynamics. USPAS Summer 2021 Spin Class Lectures. Springer (2023)
14. Méot, F.: Zgoubi Users' Guide. https://www.osti.gov/biblio/1062013-zgoubi-users-guide Sourceforge latest version: https://sourceforge.net/p/zgoubi/code/HEAD/tree/trunk/guide/Zgoubi.pdf